[5] Preradovic S, Balbin I, Karmakar NC, Swiegers GF. Multiresonator- based chipless RFID system for low-cost item tracking. *IEEE Trans Microw Theory Tech.* 2009;57(5):1411–1419.

[6] Vena A, Perret E, Tedjini S. Design of compact and auto- compensated single-layer chipless RFID tag. *IEEE Trans Microw Theory Tech.* 2012;60(9):2913–2924.

[7] Hartmann C, Hartmann P, Brown P, Bellamy J, Claiborne L, Bonner W. Anti-collision methods for global SAW RFID tag systems.IEEE Ultrasonics Symposium, 2004, Vol. 2, pp. 805–808.

[8] Nair R, Perret E, Tedjini S. Novel encoding in chipless RFID using group delay characteristics. 2011 SBMO/IEEE MTT-S International Microwave and Optoelectronics Conference (IMOC 2011), Natal, 2011, pp. 896–900.

[9] Balbin I, Karmakar NC. Phase-encoded chipless RFID transponder for large-scale low-cost applications. *IEEE Microw Wireless Compon Lett.* 2009;19(8):509–511.

[10] Zomorrodi M, Karmakar NC. Novel MIMO-based technique for EM-imaging of chipless RFID. 2015 IEEE MTT-S International Microwave Symposium, Phoenix, AZ, 2015, pp. 1–4.

[11] Agência Nacional de Telecomunicações, Resolução 506. [Online]. Available: http://www.anatel.gov.br/legislacao/resolucoes/2008/104-resolucao-506

[12] Rogers Corporation, Datasheet of Roger6010. [Online]. Available: https://www.rogerscorp.com/documents/612/acs/RT-duroid-6006-6010LM-laminate-data-sheet.pdf

[13] National Instruments, TX-LINE: Transmission Line Calculator. [Online]. Available: http://www.awrcorp.com/products/options/tx-linetransmission-line-calculator

[14] LPKF Lasers and Eletronics, Protomat S103. [Online]. Available: http://www.lpkf.com/products/rapid-pcb-prototyping/circuit-boardplotter/protomat-s103.htm

[15] Computer Simulation Technology, CST Microwave Studio. [Online]. Available: https://www.cst.com/products/cstmws

[16] Mandel C, Schler M, Maasch M, Jakoby R. "A novel passive phasemodulator based on LH delay lines for chipless microwave RFID applications. In: IEEE MTT-S Int. Microw. Workshop Series, Croatia, 2009, pp. 14.

[17] Wiesbeck W, Khny D. Single reference, three target calibration and error correction for monostatic, polarimetric free space measurements. *Proc IEEE.* 1991;79(10):1551–1558.

[18] Aliakbari H, Mallahzadeh A, Nezhad SMA. A tri-band, small size radio frequency identification tag antenna with U-shaped slots. *Microw Opt Technol Lett.* 2012;54(8):1975–1978.

How to cite this article: Di Renna RB, Corrêa CRB, Magri VPR, et al. Novel design of a compact RFID chipless tag at 860, 915 MHz, and 2.4 GHz bandwidth. *Microw Opt Technol Lett*. 2017;59:2474–2479. https://doi.org/10.1002/mop.30766

Received: 1 March 2017

DOI: 10.1002/mop.30765

Planar slot antenna with circular and vertical polarization diversity

Nicholas P. Lawrence | **Christophe Fumeaux** | **Derek Abbott**

School of Electrical and Electronic Engineering
The University of Adelaide, SA 5005, Australia

Correspondence
Nicholas P. Lawrence, School of Electrical and Electronic Engineering, The University of Adelaide, SA 5005, Australia.
Email: nicholas.lawrence@adelaide.edu.au

Abstract

This article proposes an easily manufacturable multifunction two-port planar slot antenna, radiating omnidirectional linearly polarized and broadside circularly polarized radiation patterns through a common slot in an overlapping frequency bandwidth at 5.9 GHz of 2.56%, with inter-port coupling below −45 dB.

KEYWORDS

diversity, planar, polarization

1 | INTRODUCTION

Mobile data traffic is anticipated to grow one thousand-fold over the period 2010–2020. To cope with this increase, wireless resources need to be used efficiently.[1] In this article, a two-port planar slot antenna simultaneously capable of transmitting in a monopolar mode and a broadside circularly polarized (CP) mode, with high inter-port isolation, is demonstrated. Two degenerated slot modes provide two broadside patterns with orthogonal polarizations that, with a 90° phase shift between them, can generate a CP mode through sequential feeding of antenna ports.[2] The third polarization, perpendicular to the antenna surface, is offered through inclusion of a low-profile magnetic current loop electric monopole.[3] The design offers the option to beamform in three dimensions through phased feeding techniques.[4] In [4], a wearable planar antenna providing tri-polarization diversity is demonstrated by combining an inductive loaded circular monopolar patch antenna with a microstrip annular ring.

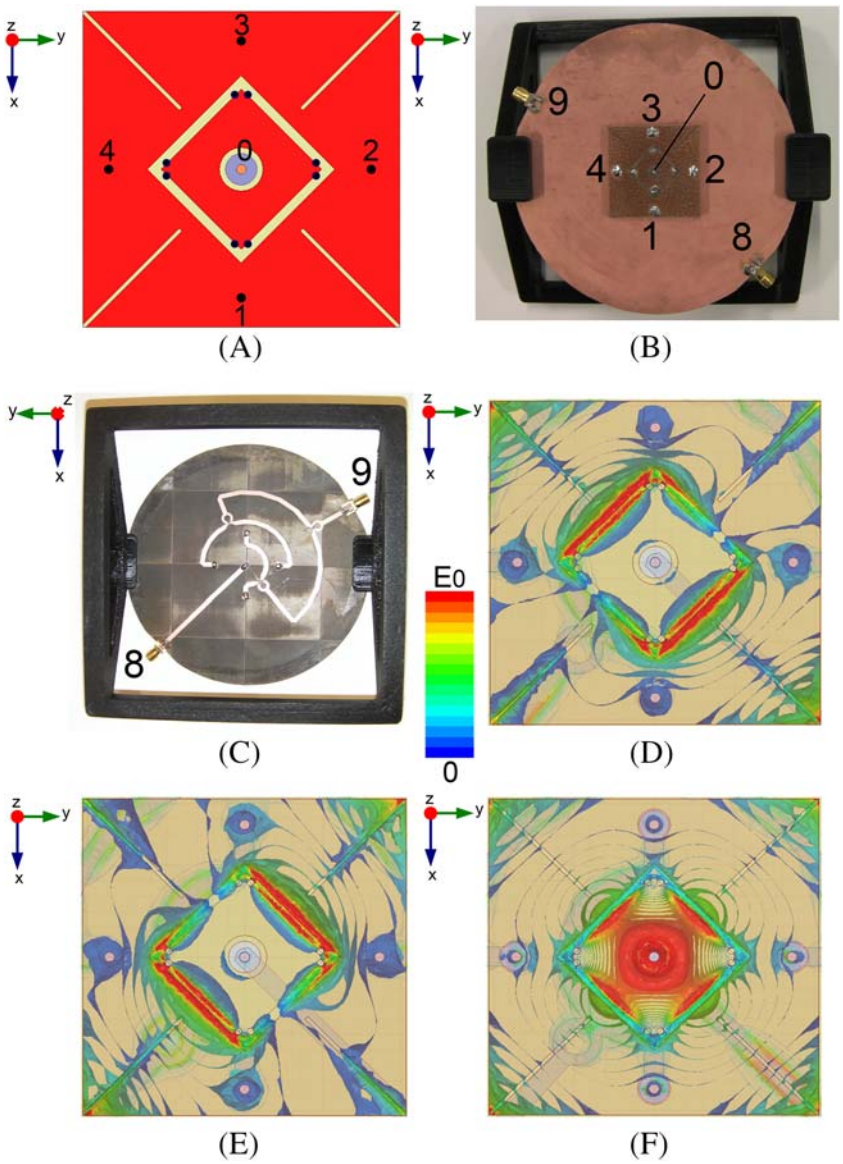

FIGURE 1 Antenna and feed design. (A) antenna, (B) manufactured antenna mounted on a ground plane, (C) manufactured feed on the back side, (D) CP mode (feed phase = 60°), (E) CP mode (feed phase = 150°), (F) monopolar mode. [Color figure can be viewed at wileyonlinelibrary.com]

The design highlighted in this paper provides a 30 dB improvement on port isolation characteristics, due to the orthogonal symmetry of a readily manufacturable square slot design. The planar antenna in this paper offers the option to beamform in three dimensions through phased feeding techniques.[5] This is demonstrated using an appropriate feeding mechanism.

2 | ANTENNA DESIGN AND FEED NETWORK

The antenna, shown in Figure 1A, consists of a square common radiative slot design allowing CP and monopolar modes to radiate from the antenna upper surface.[6] In this letter, the design is extended to offer two port reconfigurable beamforming in three dimensions through phased feeding techniques, providing additional diversity to previously demonstrated functionality. Figure 1B,C show the manufactured antenna and feed design, which are based on a 50 Ω characteristic impedance. Feed port 9 uses Wilkinson power dividers and delay lines to provide sequential feeding of antenna ports 1–4 for CP mode operation, while feed port 8 provides direct feeding of the central antenna port 0 for monopolar mode operation. Both antenna and feed are manufactured using Rogers RT Duroid 5880 material, of relative permittivity of 2.20, and of thicknesses of 3.18 and 0.79 mm, respectively. Both substrates are cladded with industry standard 17 μm of copper on either side. The antenna is square with sidelength of 41.2 mm, while the feed is 65 mm radius. Figure 1D-F illustrate the modes of operation in the antenna, namely a sequentially-fed degenerated broadside mode for CP radiation,[2] and magnetic current loop mode for monopolar radiation.

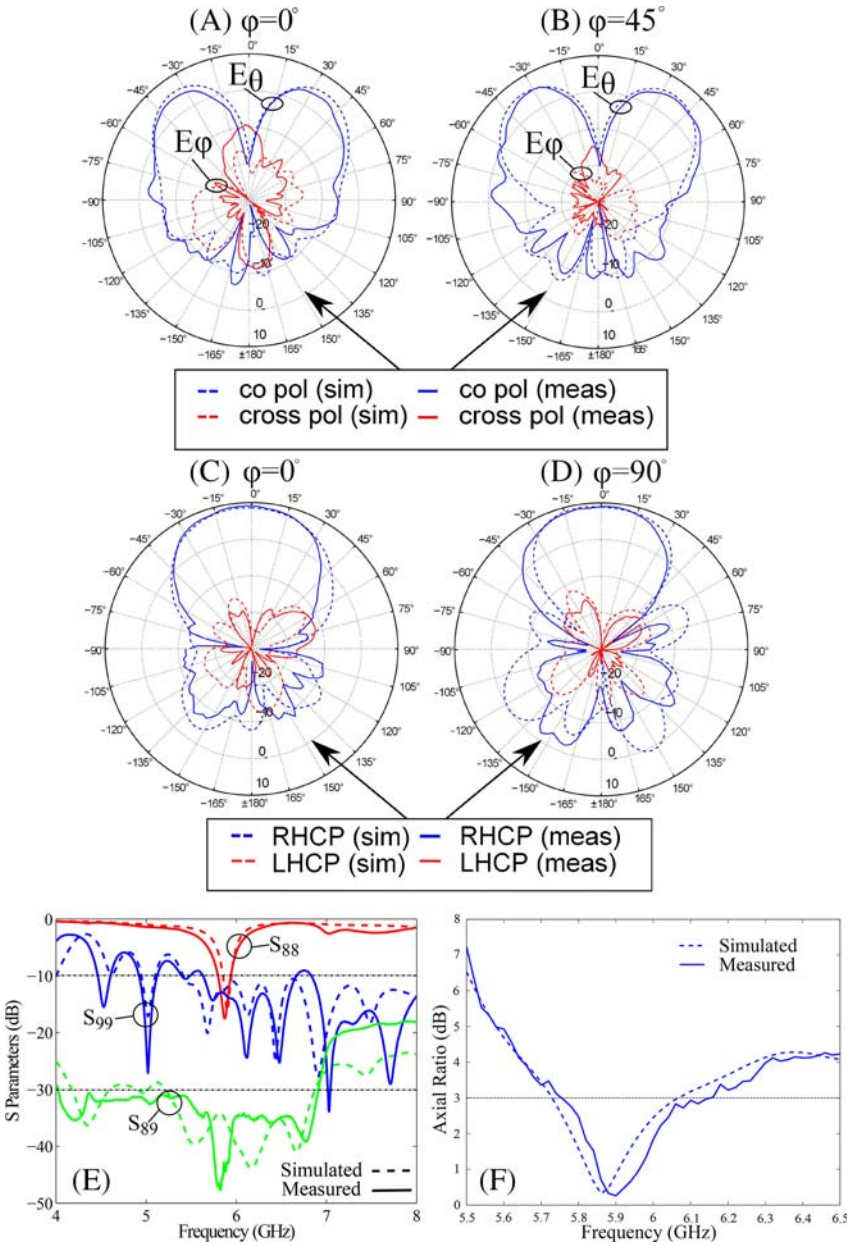

FIGURE 2 Combined antenna and monopolar, CP feed characteristics: (A,B) monopolar radiation patterns, (C,D) CP radiation patterns (E) S-parameters, (F) axial ratio. [Color figure can be viewed at wileyonlinelibrary.com]

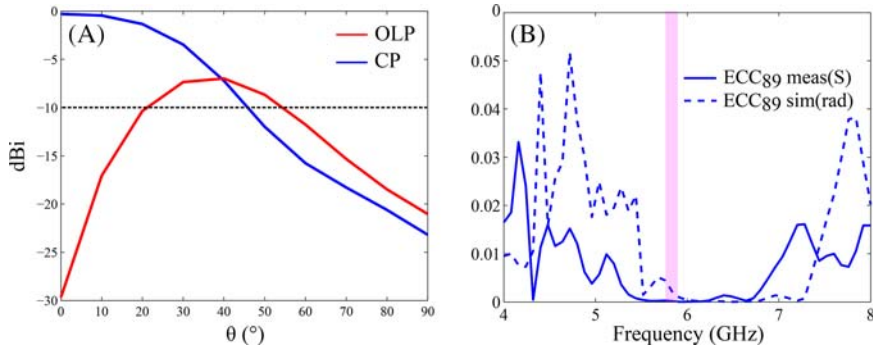

FIGURE 3 Diversity characteristics. (A) MEGs for the monopolar and CP modes in dBi as a function of θ from the zenith position, orthogonal to the antenna radiating surface, (B) measured and simulated ECCs. For convenience, the overlapping impedance bandwidth (5.79–5.94 GHz) is shown shaded. [Color figure can be viewed at wileyonlinelibrary.com]

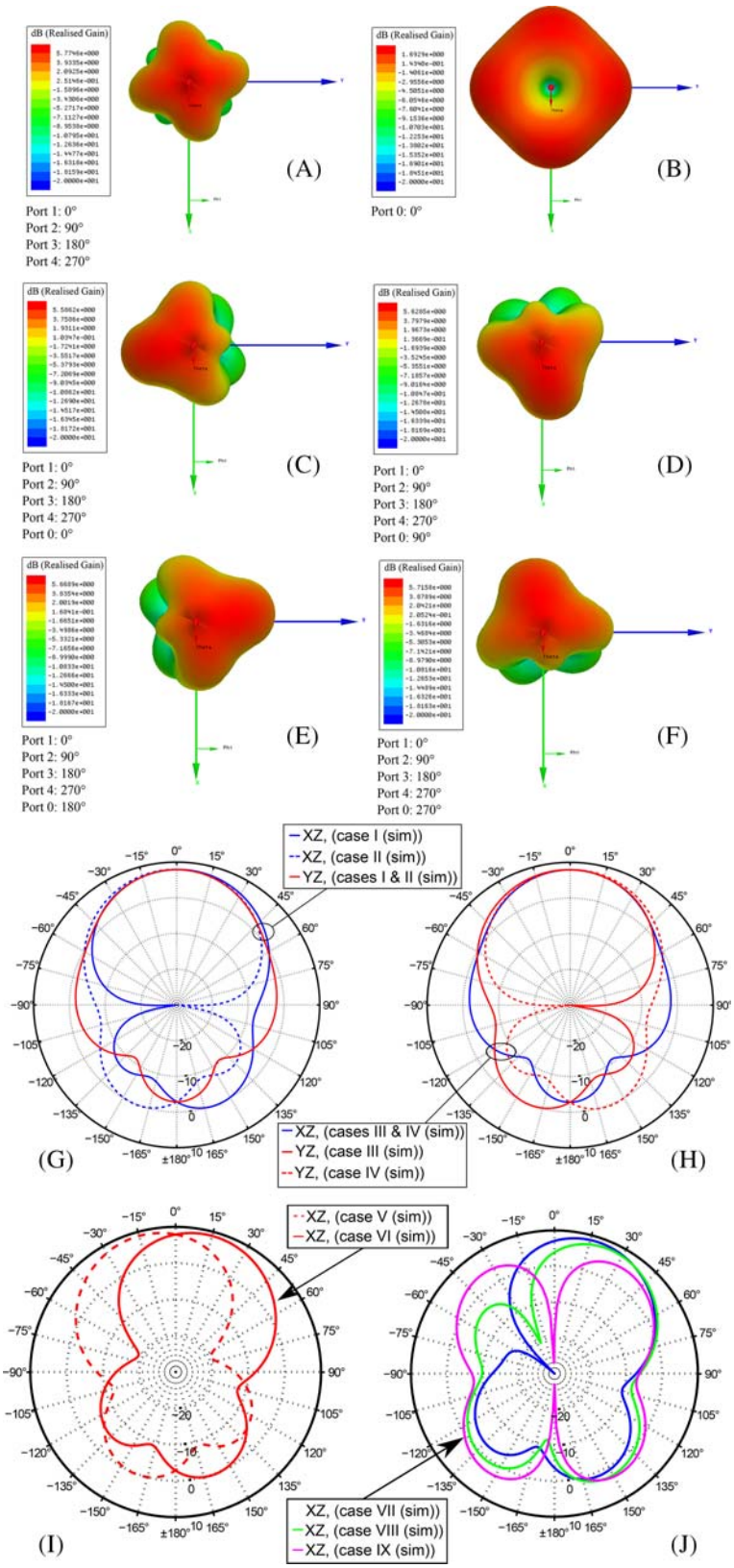

FIGURE 4 The radiation pattern of the antenna may be vector swept by exciting ports 1–4 of the CP mode while providing phase-cycled excitation of the monopolar mode through port 0. The radiation patterns shown are. (A) CP mode uniquely (B) monopolar mode uniquely, (C-F) combinations of CP mode and monopolar mode. Port diversity operation of the antenna in the XZ and YZ planes according to antenna port excitations of cases *I* to *IV* in Table I: (G) cases *I* and *II*, (H) cases *III* and *IV*. Phase and power diversity operation of the antenna in the XZ plane: (I) illustration of phase adjustment of the magnetic current loop mode excitation (cases *V* and *VI*, Table I), (J) illustration of antenna port power redistribution (cases *VII-IX*, Table 1). [Color figure can be viewed at wileyonlinelibrary.com]

TABLE 1 Diversity feeding cases, indicating fractional input power and phase at all ports

Case	Port 0	Port 1	Port 2	Port 3	Port 4
I	0.33, 0°	0.33, 180°	0	0.33, 0°	0
II	0.33, 0°	0.33, 0°	0	0.33, 180°	0
III	0.33, 0°	0	0.33, 0°	0	0.33, 180°
IV	0.33, 0°	0	0.33, 180°	0	0.33, 0°
V	0.33, 100°	0.33, 180°	0	0.33, 0°	0
VI	0.33, 280°	0.33, 180°	0	0.33, 0°	0
VII	0.50, 280°	0.25, 180°	0	0.25, 0°	0
VIII	0.80, 280°	0.1, 180°	0	0.1, 0°	0
IX	0.98, 280°	0.01, 180°	0	0.01, 0°	0

Diversity in three dimensions, through beamforming according to two port phased feeding techniques, results from polarization purity due to field cancellation of opposing sequential CP mode antenna ports, and a centrally positioned monopolar mode.[7]

3 | RESULTS

We determine three polarizations; *x*, *y*, and *z*, according to the feeding alignments shown in Figure 1. The third Ludwig definition of cross polarization is used to determine CP mode performance.[8] Simulated and measured radiation characteristics of the antenna, along with S-parameters of the monopolar, CP system and the axial ratio are illustrated in Figure 2. Simulation and measurement are observed to provide good agreement. The monopolar radiation mode provides a measured impedance bandwidth of 150 MHz, or 2.56%, centered at 5.87 GHz. A much larger CP mode impedance bandwidth is observed at 1.075 GHz (5.61–6.69 GHz), or 17.5%.

Gains of 6.4 dB in the case of magnetic current loop mode operation, and 9.3 dBiC in the case of degenerated broadside CP mode operation are measured. Back radiation is minimized, and simulated radiation efficiency is above 96%, with a worst case measured radiation efficiency of 89%. A minimum measured triorthogonal overlapping impedance bandwidth of 2.56% (5.79–5.94 GHz) is measured. In the frequency band of operation, isolation of no lower than 45 dB is measured between the operational modes.

Two commonly used criteria, the mean effective gain (MEG)[9] and the envelope correlation coefficient (ECC),[10] are utilized to evaluate the antenna diversity performance and are shown in Figure 3. Spherical integration functions of the 3D far-field antenna patterns are used to calculate both MEG and ECC metrics using a diversity model.[11] A lower MEG limit of −10 dBi and an ECC upper threshold of 0.5 are commonly held as acceptable for diversity applications. The antenna provides an extension of MEG to lower elevation angles due to the monopolar mode, as well as low correlation between modes.

An attractive option of this antenna is the ability to beamform radiation through arbitrary combinations of modes from the common radiative slot. Phase feeding techniques provide the rotating radiation pattern demonstrated in Figures 4A-F. Inclusion of amplitude adjustments provides additional radiation pattern control as shown in Figures 4G-J, according to cases *I-IX* in Table 1. Antenna port excitation is shown in the form of total input power fraction and phase according to the port numbering of Figure 1.

4 | CONCLUSION

A planar slot antenna operating at 5.9 GHz and providing monopolar and CP mode radiation is demonstrated in this paper. Measurement is in good agreement with simulation. A large ground plane would in effect provide a monopole-like magnetic current loop mode of operation, polarized orthogonally to the CP broadside mode. Control of the antenna radiation pattern is possible in three dimensions by varying feeding excitations to each of the antenna ports. Beamforming cases are highlighted. Due to a complete ground plane, low profile and straightforward manufacture, the antenna may be integrated into various systems.

CONFLICT OF INTEREST

The authors declare that they have no conflicts of interest with the contents of this article.

REFERENCES

[1] Rappaport T, Sun S, Mayzus S, Zhao R, Azar H, Wang YK, Wong GN, Schulz J, Samimi KM, Gutierrez F. Millimeter wave mobile communications for 5G cellular: It will work!. *IEEE Access.* 2013;1:335–349.

[2] Hall P, Dahele J, James J. Design principles of sequentially fed, wide bandwidth, circularly polarised microstrip antennas. *IEEE Microw Antenn Propag.* 1989;136(5):381–389.

[3] Kaufmann T, Fumeaux C. Low-profile magnetic loop monopole antenna based on a square substrate-integrated cavity. *Int J Antenn Propag*, *Article ID 694385*. 2015;

[4] Yan S, Vandenbosch GAE. Wearable antenna with tripolarisation diversity for wban communications, *Electronics Letters* 2016;52(7):500–502.

[5] Razavizadeh SM, Ahn M, Lee I. Three-dimensional beamforming: a new enabling technology for 5G wireless networks. *IEEE Sig Process Mag.* 2014;31(6):94–101.

[6] Lawrence NP, Fumeaux C, Abbott D. Planar tri-orthogonal slot antenna. *IEEE Trans Antenn Propag.* 2016;(Accepted with preprint doi:10.1109/TAP.2016.2647719).

[7] Zou L, Fumeaux C. A cross-shaped dielectric resonator antenna for multifunction and polarization diversity applications. *IEEE Antenn Wirel Propag Lett.* 2011;10:742–745.

[8] Ludwig A. The definition of cross polarization. *IEEE Trans Antenn Propag.* 1973;21(1):116–119. no. Jan

[9] Taga T. Analysis for mean effective gain of mobile antennas in land mobile radio environments. *IEEE Trans Vehicul Technol.* 1990;39(2):117–131. no. May

[10] Brown T, Saunders S, Stavrou S, Fiacco M. Characterization of polarization diversity at the mobile. *IEEE Trans Vehicul Technol.* 2007;56(5):2440–2447.

[11] Lawrence NP, Ng BW-H, Hansen HJ, Abbott D. Analysis of millimetre-wave polarization diverse multiple-input multiple-output capacity. *R Soc Open Sci.* 2015;2(12): no.

How to cite this article: Lawrence NP, Fumeaux C, Abbott D. Planar slot antenna with circular and vertical polarization diversity. *Microw Opt Technol Lett.* 2017;59:2479–2484. https://doi.org/10.1002/mop.30765

Received: 9 March 2017

DOI: 10.1002/mop.30760

A miniaturized-element bandpass frequency selective surface using meander line geometry

A. B. Varuna | Saptarshi Ghosh | Kumar Vaibhav Srivastava

Department of Electrical Engineering, Indian Institute of Technology Kanpur, Kanpur, 208016, India

Correspondence
Saptarshi Ghosh, Department of Electrical Engineering, Indian Institute of Technology Kanpur, India.
Email: joysaptarshi@gmail.com

Abstract

In this paper, a low-profile miniaturized-element frequency selective surface (FSS) is presented numerically as well as experimentally. The proposed design consists of a meandered pattern printed on both sides of an ultra-thin ($0.0005\lambda_0$) FR-4 substrate, which exhibits a bandpass characteristic at 750 MHz having unit cell dimensions of $0.017\lambda_0 \times 0.017\lambda_0$. The structure, being asymmetric in nature, selectively realizes bandpass operation for a specific polarization, whereas transmits incident wave for other polarizations. The novelties of the design lie in its miniaturization performance as well as ultra-thin profile as compared with the earlier reported structures. The proposed structure has further been analyzed through deriving equivalent circuit models and parametric variations. Finally, a prototype of the FSS is fabricated and the measured response is in good agreement with the simulated result under normal incidence.

KEYWORDS

angularly stable, bandpass filter, frequency selective surface (FSS), miniaturization

1 | INTRODUCTION

Since the past few decades, frequency selective surface (FSS) has been a subject of interest owing to its widespread applications, such as spatial filters,[1] antenna reflectors,[2] hybrid radomes,[3] absorbers,[4] high impedance surfaces,[5] and electromagnetic shields.[6] They are generally periodic structures designed to transmit, reflect and/or absorb electromagnetic (EM) waves over a desired frequency range. These FSSs are constructed by printing different metallic geometries in a periodic arrangement on either single or both sides of a dielectric substrate. Although the FSSs theoretically consist of an infinite array of structures, but practically they are limited in few numbers of periodic elements. Therefore, these FSSs should be compact in size to incorporate large number of unit cells in a given space.[7] Besides, frequency responses of miniaturized-element FSSs show less dependence on the incident angle of EM wave.[8] These lead to many researches being conducted to miniaturize the unit cell dimensions of the FSSs for yielding more accurate performances.

In the last few years, various geometries such as convoluted rings, slots, dipoles, and fractals are used to obtain miniaturized unit cells.[9–20] A periodic array of metallic loop and wire grid printed on either side of a thin substrate is presented in ref. [9] achieving miniaturization of $0.083\lambda_0$. A miniaturized FSS using lumped reactive components is shown in ref. [10], which exhibits a compact unit cell of the size $0.027\lambda_0$. The use of substrate integrated waveguide (SIW) technology to achieve compactness is also reported in ref. [11]. A 2.5-dimensional closed loop miniaturized FSS is designed in ref. [12] having unit cell dimension of $0.048\lambda_0$. A multi-layer structure has also been presented based on square-loop slots, where the unit cell size is $0.035\lambda_0$.[16] However, the unit cell dimensions can further be miniaturized as compared with these earlier reported structures.

In this letter, an ultra-thin single-layer miniaturized-element FSS has been presented based on meander line approach. The proposed structure selectively exhibits a bandpass response at 750 MHz corresponding to a unit cell dimension of $0.017\lambda_0 \times 0.017\lambda_0$, where λ_0 refers to the free